Flow Structure in Idealized Rotating Detonation Combustor with Supersonic Inflow

Ruben Fernandez
Venkat Raman
University of Michigan
Ann Arbor, MI, USA

1 Introduction

In recent years, there has been an increased interest in detonation-based propulsion due to the potential increase in thermodynamic efficiency compared to deflagration-based combustors [1]. Detonation-based combustors alleviate the need for traditional compressors, potentially reducing the required number of moving parts making them geometrically simple and lightweight [2]. The rotating detonation engine (RDE) has been extensively researched as a possible concept for achieving detonation-based propulsion. Studies have focused primarily on the rocket RDE, where fuel and oxidizer are supplied axially through separate plenums, with detailed work being done on full-scale geometries [3, 4] and simplified 2-D geometries [5, 6]. High-fidelity simulations have provided insight into the role that triple point instabilities play in the propagation of detonation waves and the complex process of stabilizing these waves [7, 8]. Studies have also found how plenum conditions affect the injector recovery time and ultimately the number of waves that are formed [9].

With the promising results and successful operation of rocket RDE designs [10], RDEs have been considered for use in an air-breathing engine cycle. This would require modifications to the RDE concept, allowing for high-speed supersonic inflow to better understanding of the flow structure observed and the impact on the operational stability. Work by Wang et al. showed the feasibility of an RDE with supersonic inflow at Mach 4 by achieving steady operation in an experimental facility [11]. Still, it did not present a clear discussion of the flow structure observed. Gupta and Schwer presented a numerical simulation of a supersonic RDE (SRDE) with inflow at Mach 2.8 showing a detailed flow structure in the SRDE [12] including the addition of an oblique detonation wave due to the supersonic inflow. Air-breathing RDE operation requires an understanding of the impact have on the inflow properties and feasibility of steady state operation. Detailed analysis of a full-scale RDE can become computationally expensive [3] and often lacks the resolution required to capture the detonation structure, with few computational cells spanning the induction length. As a result, 2-D simulations have been used to study the stability and performance of RDEs with a pressure cutoff condition [6] to model injection across the injection surface, reducing the computational cost. This work will present a modification to the pressure cutoff condition to allow supersonic injection in a 2-D RDE simulation to better understand the stability of the air-breathing RDE. Adaptive mesh refinement and the pressure cutoff condition presented are utilized to analyze the flow structure in an air-breathing RDE and study feasible operating conditions.

Correspondence to: rubenf@umich.edu

2 Numerical Methods

The simulations presented are conducted using an in-house compressible reacting flow solver [13] for the Navier-Stokes equations utilizing adaptive mesh refinement. The governing equations for the conservation of mass, energy, momentum, and mass fractions are connected using the equation of state. Convective fluxes are discretized using the Harten-Lax-van Leer-Contact (HLLC) scheme, while a central differencing scheme is used for the diffusive fluxes. This solver has been used for various detonation and RDE problems in the past [5, 9]. Finite-rate chemistry is conducted using Cantera [14] and a 9-species, 21-reaction chemistry model for hydrogen-air combustion [15].

The base grid resolution for each simulation is 468 μm in the wave-normal direction. Refinement is conducted by tagging the pressure and density gradients to refine the detonation front, oblique shocks, and contact surface. Three refinement levels are used to tag the detonation front, oblique shock, and contact surface, resulting in a resolution of 58.5 μm in the wave normal direction.

3 Geometry and Boundary Conditions

The geometry utilized in this work, as shown in Fig. 1, comes from previous work by Ullman, Schewer, and Sato [5, 6, 16]. The dimensions are 0.4788 m and 0.14 m in the x-direction and the y-direction, respectively. This is a linearized RDE where the annulus is unwrapped and periodic boundary conditions are enforced on the left and right boundaries. Premixed reactants are supplied through the bottom surface utilizing a modified pressure ratio condition derived from nozzle relations across a converging-diverging nozzle. In this formulation, the pressure ratio between the prescribed plenum pressure, P_0, and the static pressure at the boundary cell, P_{wall}, is used to compute the injection properties. The inflow conditions at each boundary cell are determined by the conditions shown below, similar to having a small injector for each cell across the injection surface modeled by a converging-diverging nozzle.

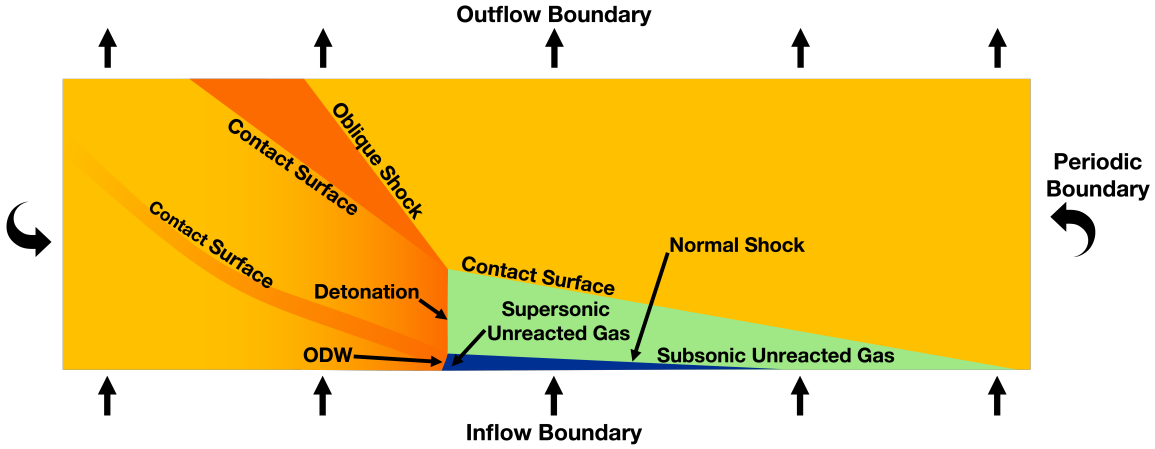

Figure 1: Schematic of geometry and boundary conditions adapted from [16].

$$\begin{aligned} P_{wall} > P_0 &\rightarrow \text{No injection,} \\ P_0 > P_{wall} > P_{cr1} &\rightarrow \text{Subsonic injection,} \\ P_{cr2} < P_{wall} < P_{cr1} &\rightarrow \text{Subsonic injection with normal shock,} \\ P_{wall} < P_{cr2} &\rightarrow \text{Supersonic injection at design conditions,} \end{aligned} \tag{1}$$

The two critical pressures, P_{cr1} and P_{cr2}, are identified as the nozzle choking pressure and the pressure when a normal shock sits at the injection surface, respectively. For each simulation, a design Mach

number, M_D, and plenum pressure, P_0, are prescribed that determine the inflow conditions and critical pressures. The Mach area relation, equation 2, is utilized to compute P_{cr1} using the design Mach number, M_D, and then finding the corresponding subsonic solution for the exit Mach number, M_{cr1}, when the flow chokes. The isentropic equation, equation 3, can then be used to compute P_{cr1}.

$$\left(\frac{A}{A^*}\right)^2 = \frac{1}{M_D^2}\left[\frac{2}{\gamma+1}\left(1+\frac{\gamma-1}{2}M_D^2\right)\right]^{(\gamma+1)/(\gamma-1)}, \tag{2}$$

$$P_{cr1} = P_0\left(1+\frac{\gamma-1}{2}{M_{cr1}}^2\right)^{\frac{-\gamma}{\gamma-1}}, \tag{3}$$

P_{cr2} is computed by first determining the post normal shock quantities, M_2 and $\frac{P_{02}}{P_{01}}$, knowing that the pre-shock Mach number, M_1, is equal to the design Mach number, M_D. Using known pressure ratios, P_{cr2} can be computed as a function of the prescribed plenum pressure and is equal to the exit pressure P_e.

$$P_{cr2} = P_0\frac{P_e}{P_{0_e}}\frac{P_{0_e}}{P_{0_2}}\frac{P_{0_2}}{P_{0_1}}\frac{P_{0_1}}{P_0}, \frac{P_{0_e}}{P_{0_2}} = \frac{P_{0_1}}{P_0} = 1, \tag{4}$$

$\frac{P_e}{P_{0_e}}$ is defined as the static pressure to total pressure ratio at the exit and is computed using the isentropic equation, equation 5.

$$\frac{P_e}{P_{0_e}} = \left(1+\frac{\gamma-1}{2}{M_2}^2\right)^{\frac{-\gamma}{\gamma-1}}, \tag{5}$$

With the critical pressures, the three flow regimes can be defined, as shown by equation 1. Inflow conditions can be specified for flow regimes as follows.

3.1 Subsonic Inflow

When subsonic inflow is experienced, the injection Mach number can be found using equation 6 where $P_{inj} = P_{wall}$.

$$M_{inj} = \sqrt{\left[\left(\frac{P_{inj}}{P_0}\right)^{-\frac{\gamma-1}{\gamma}} - 1\right]\frac{2}{\gamma-1}}, \tag{6}$$

3.2 Subsonic Inflow with Normal Shock

When a normal shock sits inside the nozzle, the inflow Mach number can be found using equation 7 as shown by Anderson [17] where $\frac{P_0}{P_{inj}}$ is the known pressure ratio and $\frac{A_e^*}{A_e}$ is the nozzle area ratio, also known by the prescribed design Mach number.

$$M_{inj} = \sqrt{-\frac{1}{\gamma-1} + \sqrt{\frac{1}{(\gamma-1)^2} + \left(\frac{2}{\gamma-1}\right)\left(\frac{2}{\gamma+1}\right)^{(\gamma+1)/(\gamma-1)}\left(\frac{P_0 A_e^*}{P_{inj}A_e}\right)^2}}, \tag{7}$$

3.3 Supersonic Injection

At design conditions, the inflow is at the design Mach number, $M_{inj} = M_D$, and the injection pressure can be found using equation 8.

$$P_{inj} = P_0 \left(1 + \frac{\gamma - 1}{2} M_D^2\right)^{\frac{-\gamma}{\gamma - 1}}, \tag{8}$$

The effects of over-expanded and under-expanded nozzles are neglected in this boundary condition definition because these effects occur after the sight of injection and would not significantly affect the properties at the injection surface. With the injection pressure and Mach number known, the injection temperature and velocity can be found using equations 9 and 10, respectively. These values are then used to compute the fluxes across the injection surface.

$$T_{inj} = T_0 \left(1 + \frac{\gamma - 1}{2} M_{inj}^2\right)^{-1}, \tag{9}$$

$$U_{inj,y} = \sqrt{\gamma R T_{inj}} * M_D, \tag{10}$$

4 Results and Discussion

To determine appropriate plenum conditions and design Mach number for an air-breathing RDE, an isentropic inlet takes the freestream conditions at 10 km to the design Mach number and the RDE plenum condition. Figure 2 shows the RDE design conditions as a function of the freestream Mach number and the intake area ratio. As expected, the plenum conditions are only a function of the freestream Mach number and result in the plenum properties increasing with the freestream Mach number.

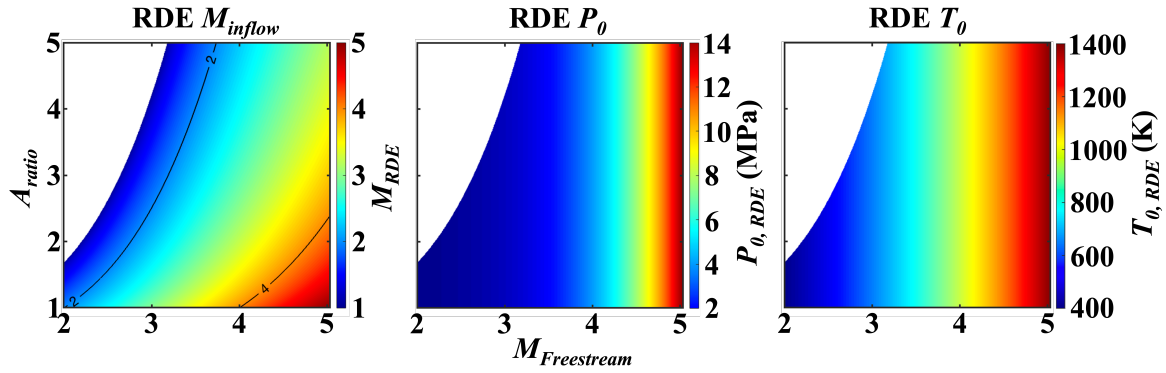

Figure 2: RDE Conditions as a function of freestream Mach number and inlet area ratio: a) Design Mach number for RDE, b) RDE plenum pressure, c) RDE plenum temperature.

This result in high plenum pressures and temperatures as the flight speed increases, which presents both benefits and challenges. As the detonation wave passes over the injector, the pressure increases at the injection surface and causes the injector being momentarily blocked until the pressure is relieved. During the recovery process, the injection velocity increases to design conditions while the injection temperature decreases from the plenum condition to the design injection temperature. As a result, injection can occur at temperatures significantly higher than injection under design conditions. For high freestream Mach numbers, the injection temperature during the recovery process can exceed the auto-ignition temperature of the fuel. This results in burning at the injector and could act as a spark in the domain leading to the formation of additional counter-rotating waves. As a result, there is a limitation to the freestream Mach number as the plenum conditions should remain below the auto-ignition temperature of the fuel. For

a stoichiometric hydrogen-air mixture, this limits the freestream Mach number to 4.03. Lower area ratio intakes could be beneficial at higher flight velocities where the RDE design Mach number would approach the freestream Mach number. Various test cases were identified from these plots, with one being highlighted in Table 4.

Table 1: Test case.

M_D	M_∞	P_0 (kPa)	T_0 (K)	A_{ratio}
3.0	3.4213	1789	743	1.50

Figure 3 below shows the steady state operation of a linearized RDE with injection at a design Mach number equal to 3. A similar flow structure can be seen as that observed by previous work [5, 6] in the case of a rocket RDE, but there are some significant differences. With supersonic injection, there is a formation of an oblique detonation wave (ODW) that sits along the injection surface and is connected to a normal detonation wave via a slip line. The unreacted gas section is also divided by a normal shock that contains supersonic unreacted gas and subsonic unreacted gas. Lastly, coming from the ODW, there is an additional contact surface that expands downstream towards the outlet, eventually interacting with the oblique shock emanating from the detonation wave. These results are in agreement with those found by Schwer and Gupta [12].

Various test cases were conducted looking at an RDE design Mach number between $2 - 4$. All test cases presented a similar flow structure as that in Fig. 3 with changes only in the infill height and the ratio of the ODW to normal detonation heights. At lower Mach numbers, the plenum pressure decreases significantly, resulting in sustained supersonic injection occurring only at a small portion of the domain. Higher plenum pressure allow for reduced injector recovery time that increases injection at design conditions. Despite this, whenever supersonic injection occurs, an ODW develops with a flow configuration as presented.

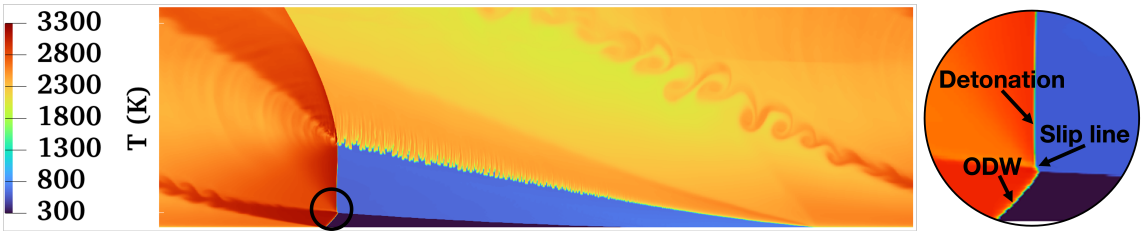

Figure 3: Steady state temperature contours with injection at Mach $= 3$ of premixed, stoichiometric hydrogen-air including zoomed in view of detonation structure (right).

5 Conclusion

In this work, the pressure cutoff conditions that are commonly used for 2-D RDE simulations are modified to achieve supersonic injection and used to determine the feasibility of an air-breathing RDE. The results show that the steady operation of an air-breathing RDE is feasible with a structure similar to that observed in a rocket RDE. Differences include the presence of an oblique detonation wave and the infill region being split into a supersonic and subsonic region by a normal shock. Steady operation was observed up to an injection Mach number equal to 4. Analysis of the RDE plenum conditions based on the freestream flight speed found increased injection temperature during the recovery process at high flight speed resulting in burning at the injectors and the creation of additional counter-rotating waves. Overall, this work presents a modified pressure cutoff condition, utilized for supersonic injection in a linearized RDE, and identified limits in flight speeds due to increased injection temperatures.

References

[1] J. Shepherd and E. Wintenberger, "Thermodynamic analysis of combustion processes for propulsion systems," in 42nd AIAA aerospace sciences meeting and exhibit, vol. 34, p. 1033, 2004.

[2] F. K. Lu and E. M. Braun, "Rotating detonation wave propulsion: experimental challenges, modeling, and engine concepts," J Propul Power, vol. 30, no. 5, pp. 1125–1142, 2014.

[3] S. Prakash, V. Raman, C. F. Lietz, W. A. Hargus Jr, and S. A. Schumaker, "Numerical simulation of a methane-oxygen rotating detonation rocket engine," P Combust Inst, vol. 38, no. 3, 2021.

[4] P. Pal, C. Xu, G. Kumar, S. A. Drennan, B. A. Rankin, and S. Som, "Large-eddy simulations and mode analysis of ethylene/air combustion in a non-premixed rotating detonation engine," in AIAA propulsion and energy 2020 forum, p. 3876, 2020.

[5] M. J. Ullman and V. Raman, "Impacts of injection scheme and grid resolution in two-dimensional rotating detonation engine simulations," in AIAA SCITECH 2024 Forum, p. 2431, 2024.

[6] D. Schwer and K. Kailasanath, "Numerical investigation of rotating detonation engines," in 46th AIAA/ASME/SAE/ASEE joint propulsion conference & exhibit, p. 6880, 2010.

[7] I. Moen, "Influence of cellular regularity on the behaviorof gaseous detonations," Dynamics of explosions, vol. 106, pp. 220–243, 1986.

[8] M. I. Radulescu and J. H. Lee, "The failure mechanism of gaseous detonations: experiments in porous wall tubes," Combust Flame, vol. 131, no. 1-2, pp. 29–46, 2002.

[9] V. Raman, S. Prakash, and M. Gamba, "Nonidealities in rotating detonation engines," Annu Rev Fluid Mech, vol. 55, no. 1, pp. 639–674, 2023.

[10] J. Sosa, R. Burke, K. A. Ahmed, D. J. Micka, J. W. Bennewitz, S. A. Danczyk, E. J. Paulson, and W. A. Hargus Jr, "Experimental evidence of h2/o2 propellants powered rotating detonation waves," Combust Flame, vol. 214, pp. 136–138, 2020.

[11] C. Wang, W. Liu, S. Liu, L. Jiang, and Z. Lin, "Experimental verification of air-breathing continuous rotating detonation fueled by hydrogen," Int J Hydrogen Energ, vol. 40, no. 30, 2015.

[12] A. K. Gupta and D. A. Schwer, "Rotating detonation engine concept: direct combustion of supersonic inflow," J Propul Power, vol. 34, no. 2, pp. 562–564, 2018.

[13] S. Sharma, R. Bielawski, O. Gibson, S. Zhang, V. Sharma, A. H. Rauch, J. Singh, S. Abisleiman, M. Ullman, S. Barwey, and V. Raman, "An amrex-based compressible reacting flow solver for high-speed reacting flows relevant to hypersonic propulsion," arXiv, 2024.

[14] D. G. Goodwin, H. K. Moffat, I. Schoegl, R. L. Speth, and B. W. Weber, "Cantera: An object-oriented software toolkit for chemical kinetics, thermodynamics, and transport processes," 2023.

[15] M. A. Mueller, T. J. Kim, R. A. Yetter, and F. L. Dryer, "Flow reactor studies and kinetic modeling of the h2/o2 reaction," Int J Chem Kinet, vol. 31, no. 2, pp. 113–125, 1999.

[16] T. Sato, S. Voelkel, and V. Raman, "Analysis of detonation structures with hydrocarbon fuels for application towards rotating detonation engines," in 2018 joint propulsion conference, 2018.

[17] J. D. Anderson, "Modern compressible flow with historical perspective 3rd edition," McGraw Hill Higher Education, pp. 1–760, 2003.